Effect of embedding nanoparticles on the lattice thermal conductivity of bulk semiconductor crystals

Younès Ezzahri, Karl Joulain

Effect of embedding nanoparticles on the lattice thermal conductivity of bulk semiconductor crystals

Younès Ezzahri and Karl Joulain

Citation: Journal of Applied Physics **113**, 043510 (2013); doi: 10.1063/1.4789808
View online: http://dx.doi.org/10.1063/1.4789808
View Table of Contents: http://scitation.aip.org/content/aip/journal/jap/113/4?ver=pdfcov
Published by the AIP Publishing

Effect of embedding nanoparticles on the lattice thermal conductivity of bulk semiconductor crystals

Younès Ezzahri[a] and Karl Joulain
Département Fluides, Thermique, Combustion, Institut Pprime, ENSIP-Bâtiment de Mécanique, CNRS-Université de Poitiers-ENSMA, 2 rue Pierre Brousse, F 86022 Poitiers Cedex, France

(Received 4 December 2012; accepted 15 January 2013; published online 25 January 2013)

We analyze the effect of embedding semiconductor nanoparticles as extrinsic phonon scattering centers on the steady-state $\kappa(0)$ and dynamical $\kappa(\Omega)$ behaviors of the lattice thermal conductivity of bulk semiconductor (SC) alloy crystals. As an example, we consider the case of Ge nanoparticles embedded in a $Si_{0.7}Ge_{0.3}$ alloy crystal host matrix. The analysis includes the study of the effect of changing the size and concentration of the nanoparticles in combination with changing the ambient temperature while all other intrinsic properties of the SC alloy crystal host matrix are kept constant. Our calculations confirm the existence of an optimal nanoparticles size that minimizes $\kappa(0)$. Depending on the ambient temperature, the optimal size either increases or decreases as a function of the nanoparticles concentration. Our calculations show also the cut-off frequency f_C of $\kappa(\Omega)$ to be very sensitive to the size and concentration of the embedded nanoparticles. For a fixed ambient temperature and nanoparticles concentration, f_C manifests a very interesting behavior as a function of the nanoparticles size. While embedding nanoparticles in SC alloy matrices reduces the steady-state $\kappa(0)$, it however tends to increase f_C of the dynamical $\kappa(\Omega)$ in comparison with intrinsic SC alloys. The study sheds light also on the fundamental role that normal processes have in treating phonon heat transfer phenomenon. © *2013 American Institute of Physics*. [http://dx.doi.org/10.1063/1.4789808]

I. INTRODUCTION

Current research in the field of thermoelectricity has proved the thermal conductivity to play a vital and the most fundamental role in increasing the dimensionless figure of merit $ZT = (\sigma S^2/\kappa)T$ of semiconductor (SC) materials where, T is the absolute temperature, σ, S, and κ are the electrical conductivity, Seebeck coefficient, and thermal conductivity of the thermoelectric SC material, respectively. Almost all reported high values of ZT have been interpreted, validated, and confirmed as mainly due to a decrease in κ of the SC material regarding its geometry and composition.[1–9] One of the most successful methods to achieve such a reduction in κ has been "*nanostructuration*" of the thermoelectric SC crystal material.[10–14] Even though, it has been difficult to beat the "*alloy limit*" in crystals without creating defects, dislocations, and voids.

Recently, a clever approach called "*Nanoparticle-in-alloy*" has been suggested to beat the alloy limit of κ in SC crystals. This approach was experimentally demonstrated in the case of ErAs nanoparticles embedded in InGaAs matrix with a 50% reduction in κ and a corresponding 100% increase in ZT.[5] Mingo *et al.*[14–16] investigated this approach with different other material combinations and found very promising results that might have huge and potential implications in SiGe-based technology in both thermoelectricity and microelectronics. The implantation of this approach is not however trivial. Nanoparticles, which could be either metallic, semimetallic or semiconductor, have to be lattice-matched with the SC alloy crystal matrix in such a way that they can be grown inside the matrix without defects and dislocations. They also need to scatter more efficiently phonons with a negligible effect on electron mobility.[14,15] In SC alloy crystals, alloy disorder scatters phonons due either to mass difference and/or size difference and/or bond strength difference. In the Rayleigh scattering regime, the scattering cross section varies as $\sigma \sim \lambda^{-4}$ where λ is the phonon wavelength. This means that short wavelength phonons are scattered much more efficiently than mid and long wavelength phonons; hence heat conduction in an alloy is mainly dominated by these latter phonons. By incorporating nanoparticles in a SC alloy crystal, mid and long wavelength phonons are also scattered which reduces the thermal conductivity below the alloy limit.[5]

Kundo *et al.*[16] analyzed and pointed out the effect of light and heavy embedded nanoparticles on the thermal conductivity κ of a SC alloy matrix using an atomistic *ab initio* Green function approach. The authors considered $Si_{0.5}Ge_{0.5}$ SC alloy with embedded Si or Ge nanoparticles and found that the effect on κ of incorporating the nanoparticles is different depending on whether the nanoparticles are relatively heavier or lighter than the hosting matrix. The calculation predicts that heavier nanoparticles (Ge) should be more efficient than lighter ones (Si) in reducing κ of $Si_{0.5}Ge_{0.5}$. The difference is due to the fact that heavy nanoparticles scatter mid and long wavelength phonons (phonons that make the largest contribution to κ) more strongly than do the light ones.

It is worth to mention that, besides acting as phonon scattering centers, embedded nanoparticles may also act as dopants donating carriers, which will reduce the needed amount of dopant impurities in the SC matrix and thus enhance the electron mobility.[17] Additionally, energy

[a]Author to whom correspondence should be addressed. Electronic mail: younes.ezzahri@univ-poitiers.fr.

dependence scattering rates of electrons are sensitive to the long range potential screening-tails of the nanoparticles which may result in an increased Seebeck coefficient.[18]

In a very recent paper, which will be quoted ***I*** hereafter,[19] we made a study of the intrinsic behavior of the dynamical lattice thermal conductivity $\kappa(\Omega)$ of bulk SC crystals. The calculation approach was based on solving Boltzmann-Peierls phonon transport equation in the frequency domain after excitation by a dynamical temperature gradient, within the framework of the single relaxation time approximation and using modified Debye-Callaway model in which both longitudinal and transverse phonon modes are included explicitly. The SC system was assumed to have a cubic symmetry and was treated as an isotropic continuum dispersionless elastic medium. The frequency and temperature dependences of anharmonic normal (N) and Umklapp (U) three-phonon scattering processes were kept the same for all SC crystals. We were able to develop a compact expression for $\kappa(\Omega)$ that captures the leading behavior and the essential features of the dynamical thermal conduction by phonons. We considered the study of the effect of ambient temperature, Grüneisen parameter as well as the mass-difference fluctuation parameter. Our calculations confirmed previous theoretical studies regarding the order of magnitude of the cut-off frequency f_C of $\kappa(\Omega)$ and further showed f_C to be very sensitive to the variation of temperature and Grüneisen parameter. On the other hand, varying the mass-difference fluctuation parameter seemed to have no significant effect on f_C. The aim of the present paper is to extend this analysis to include the effect of "*Nanoparticle-in-alloy*" approach on the behavior of $\kappa(\Omega)$ of a SC alloy matrix. The case of steady-state behavior $\kappa(0)$ is reviewed to point out the fundamental role of three-phonon N-processes in treating phonon heat transfer phenomenon. We will continue to assume the same framework and assumptions presented in ***I***. As a test SC alloy crystal, we will consider a $Si_{0.7}Ge_{0.3}$ SC alloy host matrix in which we incorporate spherical Ge nanoparticles.[14,16]

II. THEORETICAL APPROACH

In contrast with the previous study by Mingo *et al.*[14,15] in which phonon scattering N-processes were disregarded, we consider in our analysis all phonon scattering processes to be active. In this case, in addition to N-processes, we have four resistive phonon scattering processes to take into account; Umklapp scattering, alloy-disorder scattering, boundary scattering, and scattering of phonons by the embedded nanoparticles.

The previous study in ***I*** of the dynamical lattice thermal conductivity $\kappa(\Omega)$ of bulk SC crystals led to the following simple compact expression:

$$\begin{cases} \kappa(\Omega) = \sum_S \int \dfrac{\kappa^0_{q,S}}{1 - j\Omega\tau^C_{q,S}} d^3\boldsymbol{q} = \kappa_r(\Omega) + j\kappa_i(\Omega) \\ \kappa^0_{q,S} = \dfrac{1}{8\pi^3}\tau^C_{q,S}[1 + \beta_S/\tau^N_{q,S}]v^2_{S,\iota}C_{Ph}(\boldsymbol{q},S) \end{cases}, \quad (1)$$

where $C_{Ph}(\boldsymbol{q},S) = C_{Ph}(\omega_{\boldsymbol{q},S},T_0) = \hbar\omega_{\boldsymbol{q},S}dn^0_{\boldsymbol{q},S}/dT_0$ is the specific heat per normal phonon mode,[20–22] in which $\boldsymbol{q}$ is the phonon wave vector, $\omega_{\boldsymbol{q},S}$ is the dispersion relation of the phonon in state $(\boldsymbol{q}, S)$, $S = (L, T)$ refers to the phonon polarization branch, $n^0_{\boldsymbol{q},S}$ is equilibrium Planck distribution, and T_0 refers to the local equilibrium absolute temperature. $v^2_{S,\iota} = v^2_S/3$ is the square of the acoustic group velocity of the phonon in the direction $\vec{\iota}$ of the applied temperature gradient, the 1/3 factor takes into account the assumed cubic symmetry of the SC crystal (isotropy of the group velocity in the modified Debye-Callaway model).[20–22] $\tau^N_{q,S}$, β_S, and $\tau^C_{q,S}$ are the relaxation time of three-phonon N-processes, Callaway pseudo relaxation time, and the combined relaxation time, respectively. The latter is defined as $\tau^C_{q,S} = \tau^N_{q,S}\tau^R_{q,S}/(\tau^N_{q,S} + \tau^R_{q,S})$ in which $\tau^R_{q,S}$ represents the relaxation time of all resistive phonon scattering processes (three-phonon U-processes and all extrinsic processes). j is the complex operator $(j^2 = -1)$ and Ω represents the circular frequency which is related to the real frequency by the standard definition $\Omega = 2\pi f$.

In Eq. (1), κ_r and κ_i are, respectively, the real and the imaginary parts of $\kappa(\Omega)$

$$\begin{cases} \kappa_r(\Omega) = \sum_S \int \dfrac{\kappa^0_{q,S}}{1 + (\Omega\tau^C_{q,S})^2} d^3\boldsymbol{q} \\ \kappa_i(\Omega) = \sum_S \int \kappa^0_{q,S} \dfrac{\Omega\tau^C_{q,S}}{1 + (\Omega\tau^C_{q,S})^2} d^3\boldsymbol{q} \end{cases}. \quad (2)$$

To simplify more the expression of $\kappa(\Omega)$, we express it, as it is customary in the modified Debye-Callaway model, as the sum over one longitudinal (κ_L) and two degenerate transverse (κ_T) phonon polarization branches $\kappa(\Omega) = \kappa_L(\Omega) + 2\kappa_T(\Omega)$.[20–22] The total resistive scattering rate is given according to Mathienssen's rule as

$$[\tau^R_S(\omega)]^{-1} = [\tau^U_S(\omega)]^{-1} + [\tau^a_S(\omega)]^{-1} + [\tau^B_S(\omega)]^{-1} + [\tau^{np}_S(\omega)]^{-1}, \quad (3)$$

where Umklapp scattering rate τ^U_S, alloy disorder scattering rate τ^a_S, and boundary scattering rate τ^B_S are as calculated in ***I***. On the other hand, nanoparticle scattering rate is calculated by assuming a spherical shape and using a Mathienssen type interpolation between the long and the short wavelength scattering regimes[14,16,23]

$$[\tau^{np}_S(\omega)]^{-1} = \frac{v_S[\sigma^{-1}_{sS} + \sigma^{-1}_{lS}]^{-1}}{V_{np}} f_{np}, \quad (4)$$

where $V_{np} = \frac{4}{3}\pi R^3$ is the nanoparticle volume of radius R, σ_{sS}, and σ_{lS} are the cross sections of the short and long wavelength scattering regimes, respectively, and f_{np} is the nanoparticle volume fraction. Equation (4) holds in the linear regime that is valid for small values of f_{np}, which case we assume here in our treatment of $\kappa(0)$ and $\kappa(\Omega)$. The scattering cross section limits are given by[14,15,22,23]

$$\begin{cases} \sigma_{sS} = 2\pi R^2 \\ \sigma_{lS}(\omega) = \dfrac{4\pi}{9}\left(\dfrac{\rho - \rho_{np}}{\rho}\right)^2 R^6 \left(\dfrac{\omega}{v_S}\right)^4 \end{cases}, \quad (5)$$

where ρ and ρ_{np} are the densities of the host matrix material and the embedded nanoparticle, respectively. Equation (5) takes into account both phonon scattering contributions due to mass and size differences of the nanoparticles relative to the host SC matrix. Since we are treating the SC crystal as an elastic isotropic continuum medium, no much additional error would be introduced by neglecting the contribution due to bond strength differences.[14,15]

III. RESULTS AND DISCUSSION

As we mentioned at the end of the introduction, we assume in our present analysis Ge nanoparticles of density ($\rho_{Ge} \approx 5.323\ \mathrm{g/cm^3}$) to be embedded in $Si_{0.7}Ge_{0.3}$ SC alloy matrix of density ($\rho_{Si_{0.7}Ge_{0.3}} \approx 3.332\ \mathrm{g/cm^3}$). Geometrical and physical properties of these two SC materials can be found in Tables I and II of our recent paper ***I***. We assume that including the nanoparticles will not affect the intrinsic physical properties of the SC host alloy. We will first analyze the case of a fixed nanoparticle volume fraction of $f_{np} = 2\%$. We make the assumption that this value of f_{np} will not affect negatively the electron mobility.[14,15] In fact, as has been discussed by Mingo *et al.*,[14,15] the effect of nanoparticles on the electron mobility of the SC alloy matrix will be negligible if the contribution to the electron mean free path (MFP) due to this scattering process is much larger than the intrinsic MFP due to the pure inelastic alloy scattering. According to Mingo *et al.*,[14,15] the MFP of electrons due to nanoparticle scattering is given by $\ell_{np} \sim R/3f_{np}$. On the other hand, the MFP due to the pure inelastic alloy scattering is energy independent and can be estimated from the measurements of the electron mobility. Using the relation between electrical mobility and the relaxation time $\mu(T) \sim e\tau(k_BT)/m^* = e\ell_{alloy}/\sqrt{3k_Bm^*T}$,[22] the aforementioned condition to neglect the effect of nanoparticle scattering on the electron mobility becomes then

$$\ell_{np} > \ell_{alloy} \Rightarrow f_{np} < \frac{R}{3\ell_{alloy}} \sim \frac{eR}{3\mu(T)\sqrt{3k_Bm^*T}}, \qquad (6)$$

where e is the electron elementary absolute charge and m^* is the electron (hole) effective mass at the bottom of the conduction band (top of the valence band) depending on whether the SC alloy is N or P type. According to Slack and Hussain,[24] the total electron mobility in a $Si_{(1-x)}Ge_x$ SC alloy can be estimated using

$$\begin{cases} \mu(x,T_0)_{Tot}^{-1} = \mu_V^{-1} + \mu_{alloy}^{-1} \\ \mu_{alloy}(x,T_0) = \mu_0/[4x(1-x)\sqrt{T_0/300}]\ \mathrm{cm^2/Vs} \\ \mu_V(x,T_0 = 300K) = [86x + (1-x)40.7]\ \mathrm{cm^2/Vs} \end{cases}, \qquad (7)$$

where μ_{alloy} is the alloy mobility term and μ_V is the virtual crystal mobility term, T_0 is the local equilibrium absolute temperature, and $\mu_0 \sim 150$ for a N type and ~ 140 for P type SC material.[24]

At room temperature, this will give electron mobility for the $Si_{0.7}Ge_{0.3}$ SC material of about $\sim 41\ \mathrm{cm^2/Vs}$ for both N and P types. The effective mass m^* can be a complicated function of the doping level, temperature as well as the content of Ge in the $Si_{(1-x)}Ge_x$ SC alloy. For the present calculations, we take the effective mass of conductivity for both electrons and holes in $Si_{0.7}Ge_{0.3}$ SC alloy to be the same $m^* \sim m_0$ where m_0 is the free electron mass.[24] We obtain an alloy limited MFP of $\ell_{alloy} \approx 2.7\ \mathrm{nm}$. By using this value, the condition on the nanoparticle volume fraction [Eq. (6)] becomes $f_{np} < R/8\ \mathrm{nm}$. This result means that for $f_{np} = 2\%$, nanoparticles of radius R larger than 0.2 nm will not have any significant effect on the electronic MFP. This is very comforting since we are considering R to vary over an interval [1–100 nm]. We should mention here, that since the nanoparticle contribution to the electron scattering rate does not depend on temperature, the above discussion remains valid at high temperature.[14] Nevertheless, electron mobility in the low T regime might be affected.

In Figs. 1(a) and 1(b), we report, respectively, the calculated steady-state behavior of the thermal conductivity $\kappa(0)$ of $Si_{0.7}Ge_{0.3}$ alloy matrix as a function of ambient temperature T for different values of Ge nanoparticles radius R and as a function of R for different T. Also is added to both figures, the calculated behavior of $\kappa(0)$ of $Si_{0.7}Ge_{0.3}$ alloy with no nanoparticles. As we can see in Fig. 1(a), $\kappa(0)$ decreases by embedding nanoparticles and the position of the peak value tends to shift to the right by increasing R. The effect is more noticeable and even drastic in the low temperature regime where the reduction of $\kappa(0)$ can be of more than an order of magnitude and where $\kappa(0)$ continues to decrease as R increases. Furthermore, we can see that in this temperature regime, the behavior of $\kappa(0)$ tends to depart from the specific heat per unit volume T^3 power law to follow another T^r (r is some small number more likely to be rational) power law as the nanoparticle radius R increases. On the other hand, all curves seem to superimpose in the high temperature regime. In Fig. 1(b), we reproduce the same interesting feature discussed by Mingo *et al.*,[14–16] namely the existence of an optimal nanoparticle radius R_{min} that minimizes the steady-state thermal conductivity $\kappa(0)$. The existence of R_{min} is a result of the interplay between long and short wavelength scattering regimes [Eqs. (4) and (5)]. As a matter of fact, it is easy to verify from the latter equations that the nanoparticles scattering rate $[\tau_S^{np}(\omega,R)]^{-1}$ for a phonon mode at polarization S, when it is treated as a function of the nanoparticle radius R, has a maximum value $[\tau_S^{np}(\omega,R_0)]^{-1}$ for a certain radius R_0; a maximum $[\tau_S^{np}(\omega,R_0)]^{-1}$ leads to a minimum $\kappa(0)$. It is worth to mention here that due to averaging over all phonon modes, R_{min} is different from R_0. Fig. 1(b) shows also that the effect of embedding nanoparticles diminishes as T increases. In order to gain more insight onto the behavior of R_{min} as a function of T, we report in Fig. 1(c) the calculated behavior of R_{min} as a function of T; R_{min} decreases monotonically as T increases. While R_{min} is about 20 nm at $T = 3\ \mathrm{K}$, it reduces to $\sim 2\ \mathrm{nm}$ at $T = 500\ \mathrm{K}$. Nanoparticles scattering rate is temperature independent as given by Eqs. (4) and (5); the T-behavior of R_{min} can thus be understood by taking into consideration the fact that in the low T regime, the wavelength and MFP of phonons increase so that larger nanoparticles would be more effective in scattering them than smaller ones, which explains why R_{min} increases as T decreases. On the other hand, in the high T regime, scattering

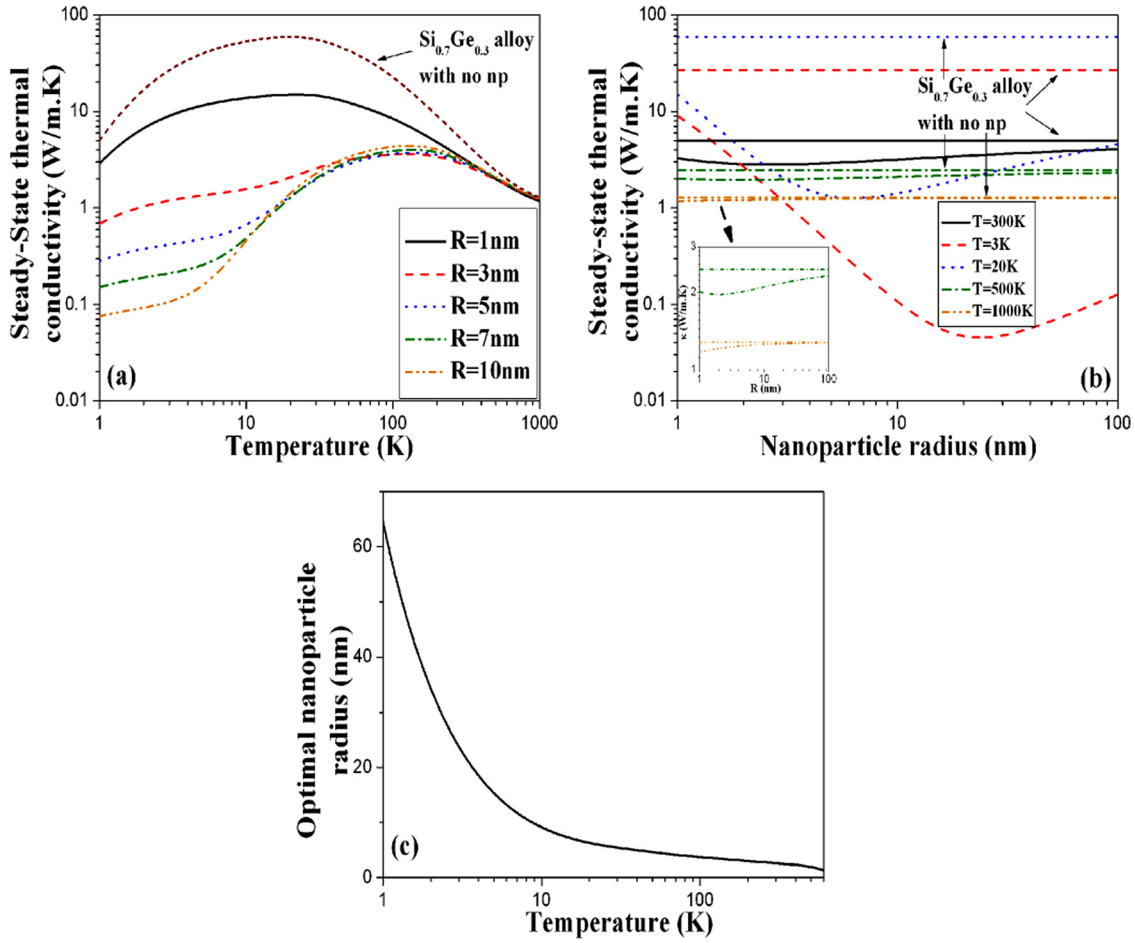

FIG. 1. Computed behaviors of $\kappa(0)$ of $Si_{0.7}Ge_{0.3}$ SC alloy with embedded Ge nanoparticles as a function of temperature T for different values of the nanoparticles radius R (a) and as a function of R for different T (b). Also are reported the values of $\kappa(0)$ of $Si_{0.7}Ge_{0.3}$ SC alloy without Ge nanoparticles. (c) Computed behavior of the optimal Ge nanoparticles radius R_{min} that minimizes $\kappa(0)$ of $Si_{0.7}Ge_{0.3}$ SC alloy as a function of T.

of phonons is due predominantly to anharmonic N-processes and U-processes so that the effect of phonon scattering by embedded nanoparticles becomes of the same order of magnitude as phonon scattering by impurities and defects in the Rayleigh regime.

The minimum of $\kappa(0)$ is very wide which is very advantageous from the technological point of view; this means that a precise control of the nanoparticles size is not essential to achieve lower thermal conductivities and consequently higher *ZTs*.

Now, let us shed some light on the dynamical behavior of $\kappa(\Omega)$. We report, respectively, in Figs. 2(a) and 2(b) the calculated room temperature dynamical behavior of the real part and the amplitude of $\kappa(\Omega)$ of $Si_{0.7}Ge_{0.3}$ SC alloy matrix with embedded Ge nanoparticles for different values of the radius R of the latter. As in the steady-state case, we added to both figures the calculated dynamical behavior of $\kappa(\Omega)$ of $Si_{0.7}Ge_{0.3}$ with no nanoparticles. There is a slight difference in the dynamical behavior with and without nanoparticles. This difference is mainly noticeable at the end of the plateau where the amplitude (real part) of $\kappa(\Omega)$ with nanoparticles seems to manifest a slight second-order-like low pass filter behavior, while the amplitude (real part) of $\kappa(\Omega)$ without nanoparticles manifests a first-order low pass filter behavior [Fig. 2(c)]. Here again, we see that in the low frequency regime, the behavior as a function of the nanoparticles radius R mirrors the steady-state behavior of $\kappa(0)$.

The effect of changing R appears on a certain intermediate range of frequency, and the high frequency f^{-1} power law in the behavior of the amplitude of $\kappa(\Omega)$ is seemingly preserved where we can see that all curves relative to different R values superimpose in the high frequency regime, this is similar to the trends we obtained in ***I*** which confirm the previous work of Volz.[25] The calculated dynamical behaviors of the imaginary part and phase of $\kappa(\Omega)$ are reported in the insets of Figs. 2(a) and 2(b), respectively. Here also, the dynamical behaviors of these two functions capture clearly the effect of changing R on $\kappa(\Omega)$. For each value of R, the imaginary part of $\kappa(\Omega)$ manifests a secondary resonance peak at the left of the primary one, the amplitudes and positions of both peaks vary by increasing R; the amplitudes vary in an opposite way; by increasing R, the amplitude of the secondary peak decreases, while the amplitude of the primary one increases. On the other hand, the positions of both peaks seem to shift left by increasing R.

We illustrate in Fig. 2(d), the calculated behavior of the cut-off frequency f_C of $\kappa(\Omega)$ of $Si_{0.7}Ge_{0.3}$ SC alloy matrix as a function of embedded Ge nanoparticles radius R for different ambient temperatures T. We report also the corresponding values of f_C of $\kappa(\Omega)$ of $Si_{0.7}Ge_{0.3}$ with no nanoparticles. f_C shows

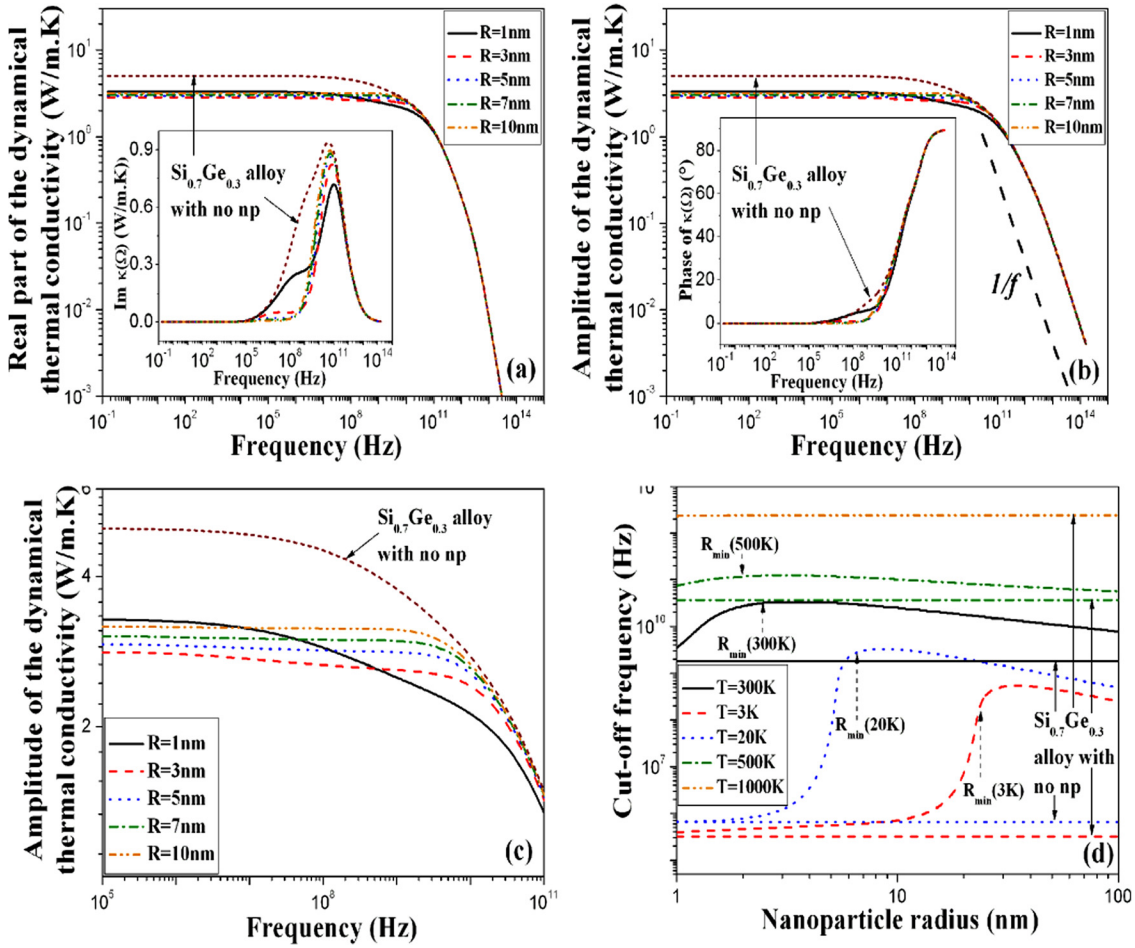

FIG. 2. Computed behaviors of the real part (a) and amplitude (b) of $\kappa(\Omega)$ of $Si_{0.7}Ge_{0.3}$ SC alloy with embedded Ge nanoparticles at room temperature as a function of frequency for different values of the nanoparticles radius R. The inset in (a) shows the imaginary part of $\kappa(\Omega)$ while the inset in (b) shows the phase. (c) A zoom of (b) over $[10^5$–10^{11} Hz] frequency interval. (d) Computed behavior of f_C of $\kappa(\Omega)$ of $Si_{0.7}Ge_{0.3}$ SC alloy with embedded Ge nanoparticles as a function of R for different T. Also are reported the values of f_C of $\kappa(\Omega)$ of $Si_{0.7}Ge_{0.3}$ SC alloy without Ge nanoparticles. The dashed arrows indicate the position of the optimal nanoparticles radius R_{min} that minimizes $\kappa(0)$ at each T.

a very interesting and curious trend that looks like a tilted step function behavior especially for low temperatures where the effect of nanoparticles scattering is more dominant. This behavior smoothes out as T is increased. In the low temperature regime, the behavior of f_C as function of R can be cast into three different regimes characterized by two threshold points; for small values of R, f_C increases slightly as R is increased. Suddenly when R reaches a certain value (first threshold point), the trend changes and f_C starts to increase faster with a higher increasing rate almost in a tilted step-like jump to reach a maximum at another larger value of R (second threshold point). After the maximum, f_C starts falling off as R is increased with a low reduction rate. Between the two threshold points, a small change in R, on the order of nanometer fluctuations, leads to a huge variation in f_C of few orders of magnitude. As T is increased, the positions of the threshold points, shift left and the steepness of f_C increasing rate between these two points tends to be less pronounced; for temperatures higher than 300 K, the first threshold point occurs for values of $R < 1$ nm. The two threshold points in the behavior of f_C as a function of R seem to correspond to values of R surrounding the optimal R_{min} value that leads to the minimum value of $\kappa(0)$ as indicated by the arrows. This behavior is again a manifestation of the interplay between long and short wavelength scattering regimes [Eqs. (4) and (5)] as mentioned previously. Investigation of Fig. 2(d) shows that for all temperatures and over the range of R values [1–100 nm], f_C of $\kappa(\Omega)$ with embedded nanoparticles is higher than the corresponding f_C of $\kappa(\Omega)$ without nanoparticles; this effect is expected since by incorporating nanoparticles, one increases the total phonon scattering rate. The average difference decreases as T gets higher, where we can see that for $T = 1000$ K, f_C of $\kappa(\Omega)$ becomes insensitive to R. This behavior corroborates the fact that in the high T regime, scattering of phonons is mainly dominated by anharmonic phonon-phonon scattering processes as we have seen in ***I***.[20–22]

Let us now see what happens when one changes the nanoparticles volume fraction f_{np} at different ambient temperatures T. As we mentioned earlier, in the high f_{np} regime, the nanoparticle scattering rate is no longer linear to f_{np} due essentially to multiple scattering effects. Besides, a high nanoparticles concentration may lead to undesirable additional scattering of electrons in the SC matrix, hence negatively affecting the electron mobility.[14]

In our case, we assume f_{np} to vary from 1% to 10% and we continue to make the hypothesis of a linear relation

linking the nanoparticle scattering rate and f_{np} [Eq. (4)]. For a maximum value of $f_{np} = 10\%$, the effect of nanoparticles on the electronic MFP would be negligible if their radius R is larger than 0.8 nm. This condition is still fulfilled regarding the interval of variation of R. Embedding Ge nanoparticles with f_{np} varying from 1% to 10% will continue to affect mainly phonon transport.

We report in Figs. 3(a)–3(c) the calculated steady-state behaviors of $\kappa(0)$ of $Si_{0.7}Ge_{0.3}$ SC alloy matrix as a function of the embedded Ge nanoparticles radius R for different values of the nanoparticles volume fraction f_{np} at $T = 3$ K, 20 K, and 500 K, respectively. As these figures show, at each ambient temperature, $\kappa(0)$ decreases as f_{np} is increased; an expected effect regarding the proportionality between the nanoparticle scattering rate and f_{np} [Eq. (4)]. For each value of R, the decreasing rate is higher at low T and tends to decrease as T increases. Besides, we can see that the position of the optimal nanoparticles radius R_{min} that leads to the minimum $\kappa(0)$ shifts either right or left depending on the value of T. While in the low T regime, R_{min} increases by increasing f_{np} (right shift), this tendency reverses as T increases where we can see that for both $T = 20$ K and $T = 500$ K, R_{min} decreases by increasing f_{np} (left shift).

These results are confirmed in Figs. 4(a) and 4(c) that report, respectively, the calculated behavior of R_{min} as a function of T for different values of f_{np} and as a function of f_{np} for different values of T. In these figures, around $T_i = 10$ K appears to be the inversion temperature region, below which R_{min} increases as a function of f_{np} and above which R_{min} decreases as a function of f_{np}. These figures show also that in both T regimes, the rate of increasing or decreasing of R_{min} as a function of f_{np}, increases by further decreasing or increasing T.

If it is straightforward to explain the behavior of R_{min} as a function of T for a fixed f_{np} due to the interplay between extrinsic and intrinsic phonon scattering processes depending on the T regime, on the other hand understanding of the interesting behavior of R_{min} as function of f_{np} at different T is seemingly not trivial regarding the assumptions made, particularly the linearity between the nanoparticles scattering rate and f_{np}. The latter assumption forbids any multiple scattering effects.

In Figs. 4(b) and 4(d), we report, the calculated minimum of $\kappa(0)$ as a function of T for different values of f_{np} and as a function of f_{np} for different values of T, respectively. Min[$\kappa(0)$] as a function of T manifests an almost Gaussian-like shape with a peak amplitude (position) that decreases (increases) by increasing f_{np}. It is seen also that the variation around the peak gets wider as f_{np} increases. On the other hand, Fig. 4(d) shows that Min[$\kappa(0)$] decreases by increasing

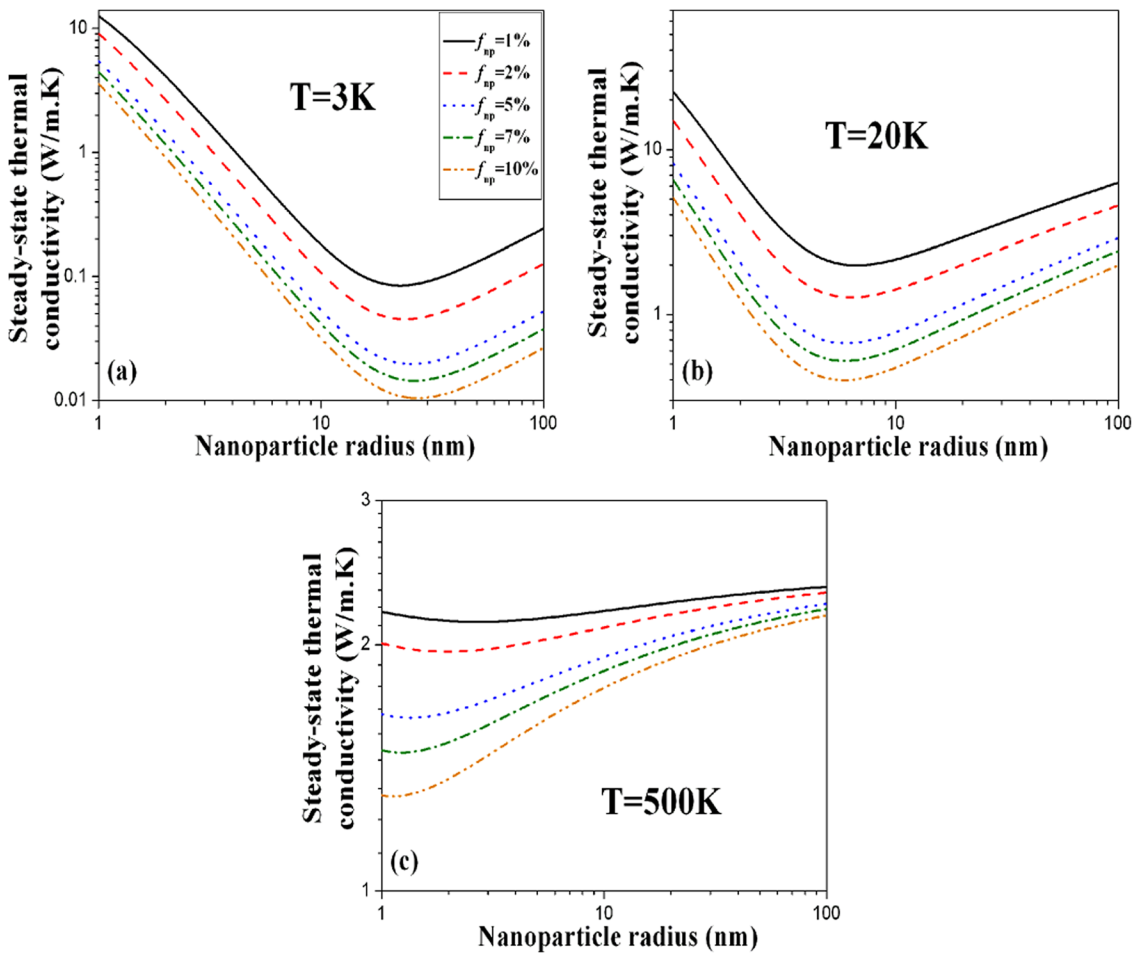

FIG. 3. Computed behaviors of $\kappa(0)$ of $Si_{0.7}Ge_{0.3}$ SC alloy with embedded Ge nanoparticles as a function of the nanoparticles radius R for different values of the nanoparticles volume fraction f_{np} at: (a) $T = 3$ K, (b) $T = 20$ K, and (c) $T = 500$ K.

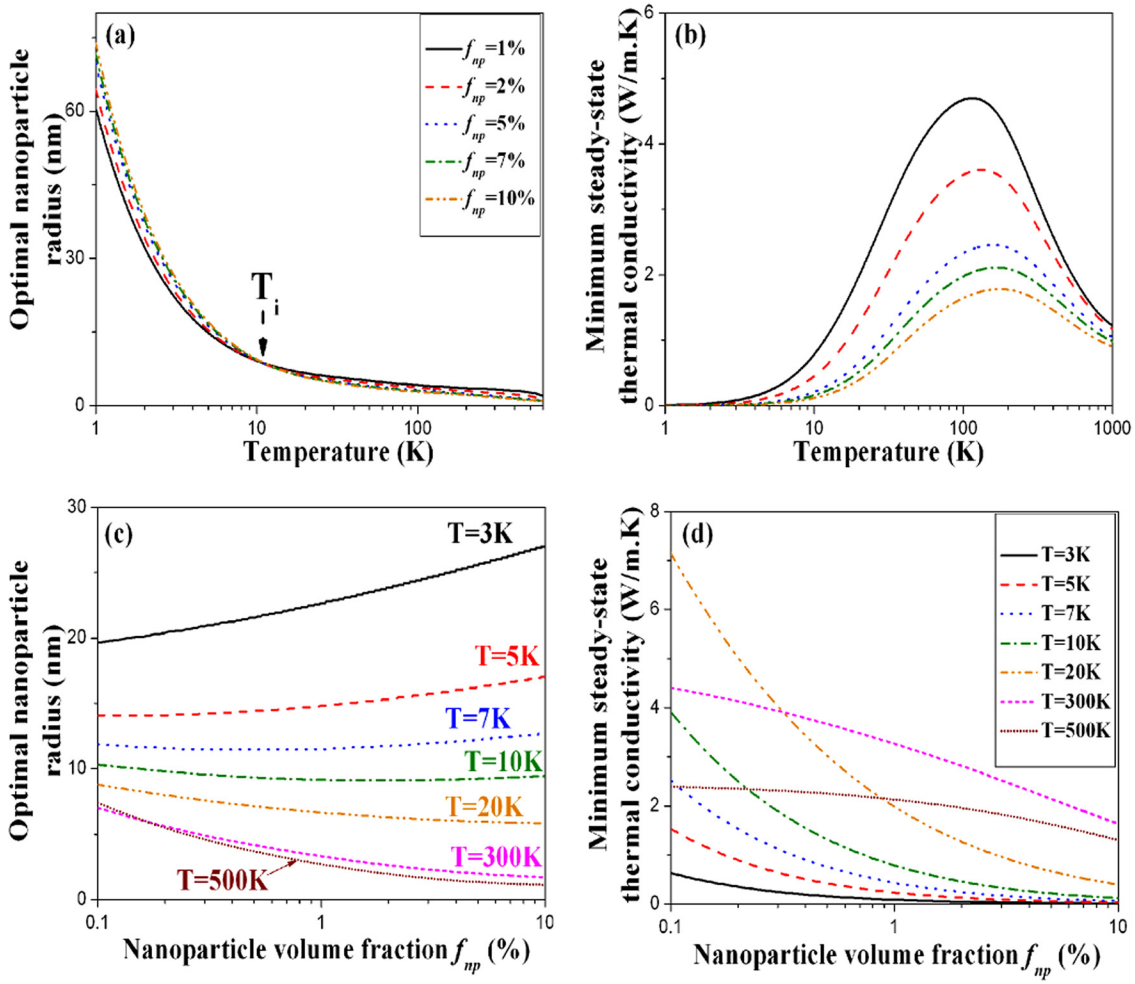

FIG. 4. Computed behaviors of the optimal Ge nanoparticles radius R_{min} [(a) and (c)] and the corresponding minimum of $\kappa(0)$ [(b) and (d)] of $Si_{0.7}Ge_{0.3}$ SC alloy as a function of T and f_{np} for different values of f_{np} and T. The arrow in (a) points the inversion temperature region at which the behavior of R_{min} as a function of f_{np} switches. This is confirmed in (c) (see text for description).

f_{np} in a monotonic way that tends to saturate however by increasing the ambient temperature T when embedding nanoparticles become less effective.

The calculated dynamical behaviors of the amplitude and imaginary part of $\kappa(\Omega)$ of $Si_{0.7}Ge_{0.3}$ SC alloy matrix with embedded Ge nanoparticles are reported in Figs. 5(a)–5(c) at $T = 3\,K$, $T = 20\,K$, and $T = 500\,K$, respectively, for different values of f_{np} and corresponding values of R_{min} that lead to Min[$\kappa(0)$] [Figs. 3 and 4]. While in the low frequency regime, the amplitude of $\kappa(\Omega)$ decreases by increasing f_{np} as expected, all other features seem to be preserved as discussed in Fig. 2. All the curves seem to collapse in the high frequency regime where the f^{-1} power law continues to be valid. The dynamical behavior of the imaginary part of $\kappa(\Omega)$ is reported in the insets of Fig. 5. The imaginary part manifests a double resonance peaks; a primary one at the right and a secondary one at the left. In the high T regime where scattering of phonon by nanoparticles becomes less significant, the secondary peak disappears and only remains the primary one, the position of which shifts to the right by increasing f_{np}. In the low T regime, the amplitude of both peaks decreases by increasing f_{np}, while their positions seem to shift to the right also.

The last figure relative to the effect of changing f_{np} on the behavior of $\kappa(\Omega)$ of $Si_{0.7}Ge_{0.3}$ SC alloy matrix with embedded Ge nanoparticles is Fig. 6. The latter reports the behavior of the cut-off frequency f_C of $\kappa(\Omega)$ as a function of the nanoparticles radius R for different values of f_{np} and at different ambient temperatures $T = 3\,K$ [Fig. 6(a)], $T = 20\,K$ [Fig. 6(b)], and $T = 500\,K$ [Fig. 6(c)]. These figures show the same interesting behaviors as the ones discussed in Fig. 2(d). In addition, we can see in the low T regime [Fig. 6(a)] that the behavior of f_C as function of f_{np} goes through three different regimes that correspond somehow to the previously discussed three regimes of the behavior of f_C as a function of R [Fig. 2(d)]. f_C seems to increase a little by increasing f_{np} for values of R smaller than the lowest threshold value R_1, then the tendency reverses when R becomes between R_1 and R_2. Once R becomes higher than R_2, f_C returns to its first tendency and starts to increase as f_{np} increases. Analyzing Fig. 6 shows also that by increasing f_{np}, the position of the highest threshold value R_2 shifts to the right at low T while it tends to shift to the left at high T. This behavior is deeply connected to the interesting behavior of R_{min} of steady-state $\kappa(0)$ as function of f_{np} for different ambient temperatures.

This intriguing, yet very interesting behavior, of f_C as function of embedded nanoparticles radius R and nanoparticles volume fraction f_{np}, shows clearly how sensitive the dynamical behavior of $\kappa(\Omega)$ could be to the nanoparticles size

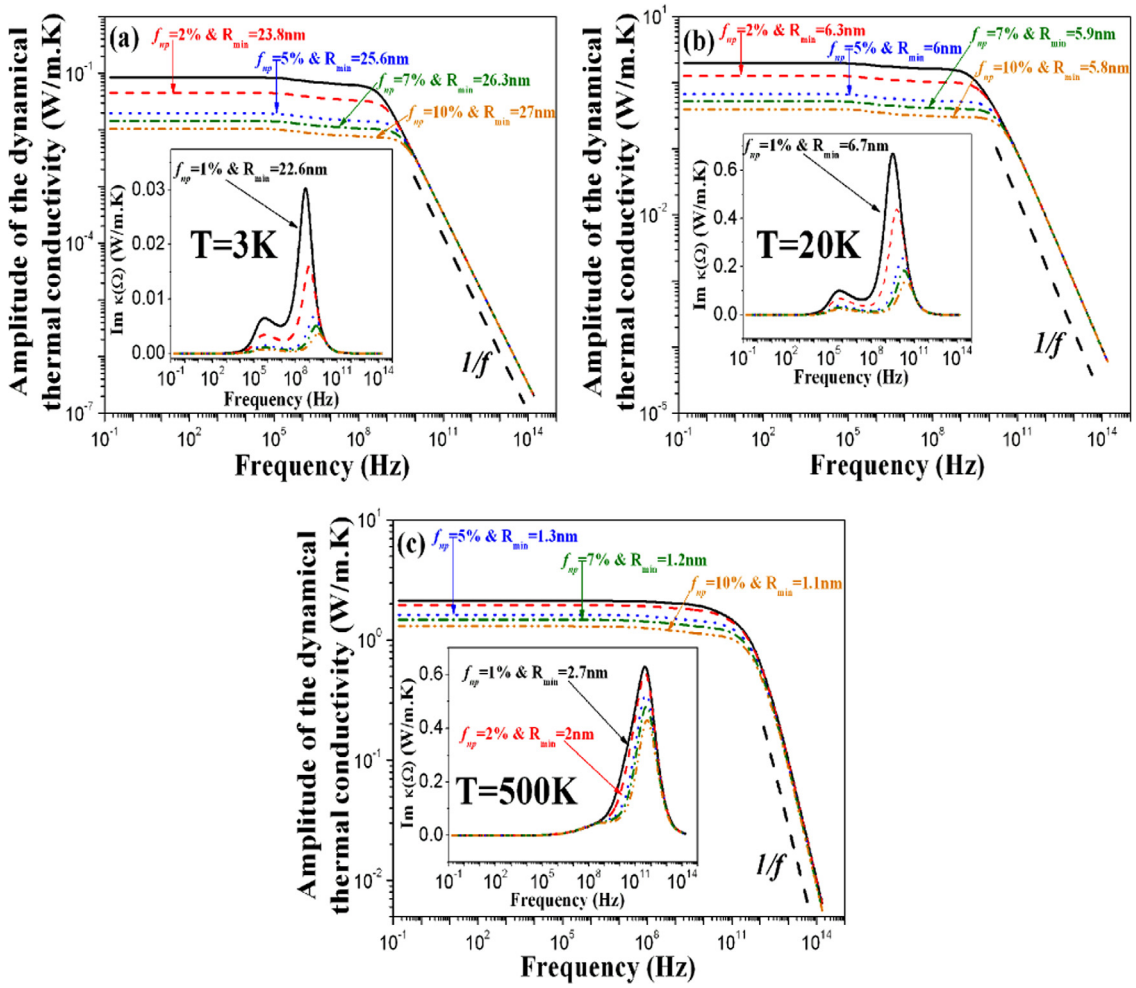

FIG. 5. Computed behaviors of the amplitude and imaginary part (inset) of $\kappa(\Omega)$ of $Si_{0.7}Ge_{0.3}$ SC alloy with embedded Ge nanoparticles as a function of frequency for different values of f_{np} and corresponding R_{min} at (a) $T = 3$ K, (b) $T = 20$ K, and (c) $T = 500$ K.

and concentration. It shows that a crucial and careful manipulation of the nanoparticles size and concentration is needed in order to adjust f_C to the expected range, especially for nanoparticles engineered and grown with sizes that surround the optimal size leading to the minimum value of $\kappa(0)$. Generally speaking, while embedding nanoparticles in SC alloy matrices reduces the steady-state $\kappa(0)$, it however tends to increase f_C of the dynamical $\kappa(\Omega)$ in comparison with intrinsic SC alloys. This opposite double effect could be very beneficial in many microelectronic and optoelectronic devices.

To end this subsection, we report, respectively, in Figs. 7(a) and 7(b) a comparison between the calculated steady-state $\kappa(0)$ and the calculated f_C of the dynamical $\kappa(\Omega)$ of $Si_{0.7}Ge_{0.3}$ SC alloy matrix as a function of the embedded Ge nanoparticles radius R at different ambient temperatures T, in two cases where three-phonon scattering N-processes are considered or disregarded. As these figures show, the effect of including N-processes is insignificant in the low T regime where phonon scattering is dominated by extrinsic processes, the calculated curves totally superimpose. On the other hand, in the high T regime, where anharmonic phonon-phonon scattering processes dominate, it is crucial to include N-processes. By disregarding these processes, both values of the optimal R_{min} and the minimum $\kappa(0)$ increase, while the value of the cut-off frequency f_C of $\kappa(\Omega)$ decreases. Depending on the nanoparticle size, a change of few factors can be expected in $\kappa(0)$, while f_C can vary by one to few orders of magnitude.

Based on this short analysis within the frame work of Boltzmann-Peierls theory of phonon transport using the single relaxation time approximation with Callaway approximated form of the collision operator, embedding SC nanoparticles seems to considerably affect the dynamics of phonon heat transport in the host SC matrix depending on temperature, size, and concentration of the nanoparticles. N-processes appear also to play a very fundamental role in capturing this dynamics of energy (heat) transport in SC crystal materials. Through their role of shuffling the total phonon crystal momentum between different phonon states, N-processes have always to be considered in any study of phonon transport.

These very interesting results regarding the effect of embedding SC nanoparticles on phonon transport phenomena in SC host crystal matrices need to be checked and confirmed using experiments combined to more elaborate and sophisticated modeling of energy and heat transport in these dielectric materials using first principles calculations and atomistic *ab initio* Green function approaches.[26,27]

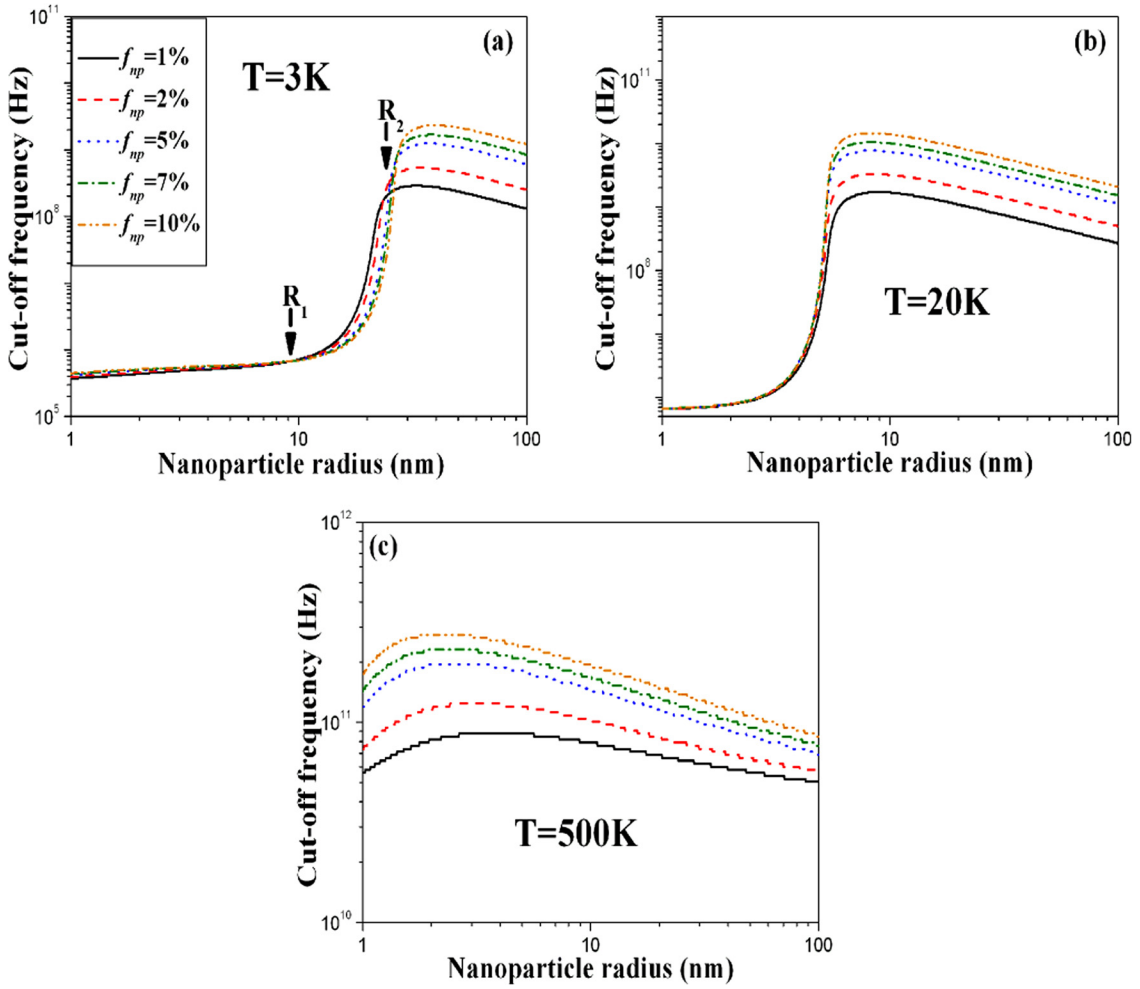

FIG. 6. Computed behaviors of f_C of $\kappa(\Omega)$ of $Si_{0.7}Ge_{0.3}$ SC alloy with embedded Ge nanoparticles as a function of R for different values of f_{np} at (a) $T = 3$ K, (b) $T = 20$ K, and (c) $T = 500$ K. The arrows on (a) point the two threshold values of R at which the behavior of f_C as function of f_{np} switches (see text for description).

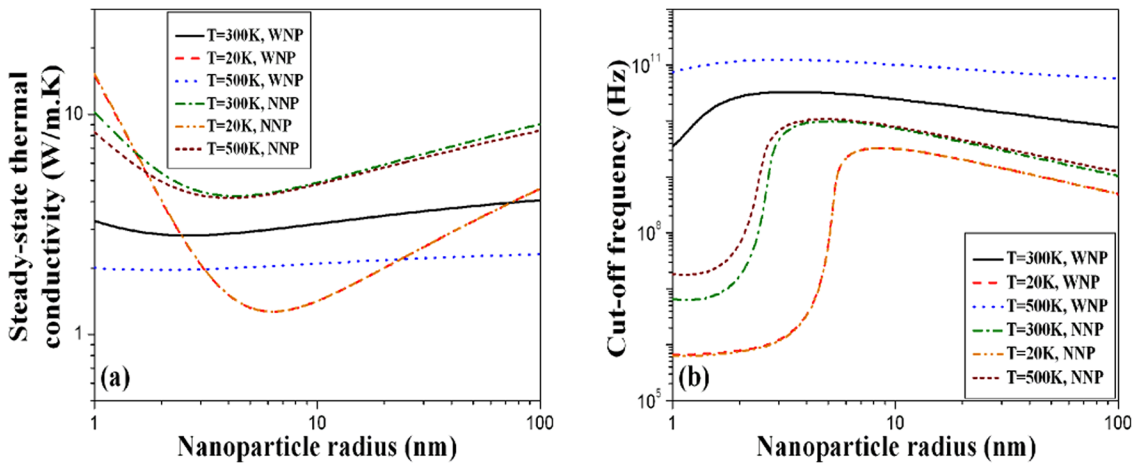

FIG. 7. (a) Computed behaviors of $\kappa(0)$ of $Si_{0.7}Ge_{0.3}$ SC alloy with embedded Ge nanoparticles as a function of the nanoparticles radius R for different T. (b) Computed behaviors of f_C of $\kappa(\Omega)$ of $Si_{0.7}Ge_{0.3}$ SC alloy with embedded Ge nanoparticles as a function of R for different T. In both figures $f_{np} = 2\%$ and we consider two cases; with (WNP) and without (NNP) three-phonon scattering N-processes.

IV. SUMMARY

We extended in this paper our previous work on the dynamical lattice thermal conductivity of bulk SC crystals to include the effect of embedding SC nanoparticles. The present analysis assumed spherical Ge nanoparticles to be embedded in a $Si_{0.7}Ge_{0.3}$ SC alloy crystal matrix. We considered the study of the effect of varying the size and concentration of the nanoparticles in addition to changing the ambient temperature. On the other hand, all other parameters of the

SC alloy crystal are kept constant. While embedding nanoparticles in SC alloy matrices reduces the steady-state $\kappa(0)$, it however tends to increase the cut-off frequency f_C of the dynamical $\kappa(\Omega)$ in comparison with intrinsic SC alloys. This opposite double effect could be very beneficial in many microelectronic and optoelectronic device applications. The behavior of $\kappa(0)$ and f_C of $\kappa(\Omega)$ as a function of the nanoparticles size and concentration revealed very interesting trends that show how important is a careful manipulation of the nanoparticles size and concentration for a better control of phonon heat transport in SC crystal alloys. The study showed also the N-processes to be indispensible and play a very fundamental role in both the steady-state and dynamical phonon transport regimes.

ACKNOWLEDGMENTS

We are grateful to Professor Ali Shakouri for his stimulating and fruitful discussions throughout this work.

[1]M. D. Row, *Handbook of Thermoelectrics* (CRC, Boca Raton, FL, 1995).
[2]G. S. Nolas, J. Sharp, and J. Goldsmid, *Thermoelectrics: Basic Principles and New Materials Developments* (Springer-Verlag, Berlin, 2002).
[3]R. Venkatasubramanian, E. Silvola, T. Colpitts, and B. O'Quinn, Nature **413**, 597 (2001).
[4]T. C. Harman, P. J. Taylor, M. P. Walsh, and B. E. Laforge, Science **297**, 2229 (2002).
[5]W. Kim, J. Zide, A. Gossard, D. Klenov, S. Stemmer, A. Shakouri, and A. Majumdar, Phys. Rev. Lett. **96**, 045901 (2006).
[6]B. Poudel, Q. Hao, Y. Ma, Y. C. Lan, A. Minnich, B. Yu, X. Yan, D. Z. Wang, A. Muto, D. Vashaee, X. Y. Chen, J. M. Liu, M. S. Dresselhaus, G. Chen, and Z. F. Ren, Science **320**, 634 (2008).
[7]A. I. Hochbaum, R. Chen, R. D. Delgado, W. Liang, E. C. Garnett, M. Najarian, A. Majumdar, and P. Yang, Nature **451**, 163 (2008).
[8]A. Shakouri, Annu. Rev. Mater. Res. **41**, 399 (2011).
[9]M. Zebarjadi, K. Esfarjani, M. S. Dresselhaus, Z. F. Ren, and G. Chen, Energy Environ. Sci. **5**, 5147 (2012).
[10]W. S. Capinski, H. J. Maris, T. Ruf, M. Cardona, K. Ploog, and D. S. Katzer, Phys. Rev. B **59**, 8105 (1999).
[11]R. Venkatasubramanian, Phys. Rev. B **61**, 3091 (2000).
[12]D. Li, Y. Wu, P. Kim, L. Shi, P. Yang, and A. Majumdar, Appl. Phys. Lett. **83**, 2934 (2003).
[13]M. L. Lee and R. Venkatasubramanian, Appl. Phys. Lett. **92**, 053112 (2008).
[14]N. Mingo, D. Hauser, N. P. Kobayashi, M. Plissonier, and A. Shakouri, Nano. Lett. **9**, 711 (2009).
[15]S. Wang and N. Mingo, Appl. Phys. Lett. **94**, 203109 (2009).
[16]A. Kundo, N. Mingo, D. A. Broido, and D. A. Stewart, Phys. Rev. B **84**, 125426 (2011).
[17]M. Zebarjadi, K. Esfarjani, A. Shakouri, J. H. Bahk, Z. Bian, G. Zeng, J. Bowers, H. Lu, J. Zide, and A. Gossard, Appl. Phys. Lett. **94**, 202105 (2009).
[18]S. V. Faleev and F. Leonard, Phys. Rev. B **77**, 214304 (2008).
[19]Y. Ezzahri and K. Joulain, J. Appl. Phys. **112**, 083515 (2012).
[20]J. Callaway, Phys. Rev. **113**, 1046 (1959).
[21]P. Carruthers, Rev. Mod. Phys. **33**, 92 (1961).
[22]J. M. Ziman, *Electron and Phonons* (Oxford University Press, New York, 1960).
[23]W. Kim and A. Majumdar, J. Appl. Phys. **99**, 084306 (2006).
[24]G. A. Slack and M. A. Hussain, J. Appl. Phys. **70**, 2694 (1991).
[25]S. Volz, Phys. Rev. Lett. **87**, 74301 (2001).
[26]K. Esfarjani, G. Chen, and H. T. Stokes, Phys. Rev. B **84**, 085204 (2011).
[27]W. Li, N. Mingo, L. Lindsay, D. A. Broido, D. A. Stewart, and N. A. Katcho, Phys. Rev. B **85**, 195436 (2012).